March 6, 2025

On the determination of the speed of a fast solar wind stream using two independent measurements of the interplanetary magnetic field.

M. J. Birch

Jeremiah Horrocks Institute for Mathematics, Physics and Astronomy,

University of Central Lancashire, Preston, UK.

Abstract

The fast solar wind stream which resulted from the helio-meridional crossing of an equatorial coronal hole during June 29th and 30th 2005 passed the Wind and ACE spacecraft during July 1st and 2nd. This fast stream caused a moderate magnetospheric storm following a weak (though clearly defined) sudden commencement at 14:12 UT on July 1st. During the event the two spacecraft were both in the vicinity of the L1 libration point, though separated in the Sun-Earth direction by about 150000 km. An algebraic method is described whereby the speed of the particle flux can be determined using measurements of the interplanetary magnetic field at the two spacecraft.

1 Introduction

Scientific study of the solar wind first began with the work of S. Chapman and V.C.A. Ferraro (Chapman, 1928; Chapman & Ferraro, 1929; Ferraro, 1933), who suggested that it comprises streams of 'corpuscles' ejected by the Sun, which reach the Earth a day or so later. Biermann (1951) studied comet tails and concluded that electromagnetic radiation pressure was insufficient to account for the observations, that the stream of corpuscles actually comprised particles, that it was continually present, and that the velocity was about 500 km.s^{-1} (a surprisingly good estimate). Subsequent studies by Parker (1958) and Chapman & Aller (1959) proved that, unlike the Earth's atmosphere, the solar corona is not in hydrostatic equilibrium but instead expands continually, with matter streaming out into the heliosphere in the form of a *solar wind*.

The continuity of the solar wind was firmly established by Mariner-2 during its flight to Venus in 1962, when it recorded alternating dense, low-speed (300-500 km.s^{-1}) and tenuous high-speed (500-800 km.s^{-1}) streams (Snyder, 1964). This finally confirmed that the solar wind is a permanent feature of the solar system. Ulysses, launched in 1990 to measure the interplanetary magnetic field (IMF) between 1.35 and 5.4 AU, was the first spacecraft to measure the solar wind at all heliolatitudes. It was also the first to confirm that the solar wind is bimodal in nature, having slow and fast components (Balogh et al., 1992).

It is now well known that the fast solar wind emerges primarily from coronal holes and expands to fill the majority of the heliospheric volume with speeds from 450 to 900 km/s (Cranmer, 2002; Cranmer, 2009; Lukianova et al., 2017), whereas the slow component (250 to 450 km/s) is associated with coronal streamers (Einaudi et al., 1999; Ofman, 2004) and may also have contributions arising from boundary flow along current sheets, the magnetic reconnection of closed-field loops, and the boundaries of coronal holes (Bravo and Stewart, 1997). The passage of low-latitude coronal holes across the helio-meridian often results in weak to moderate

magnetic storms within geospace (Sulistiani and Herdiwijaya, 2019; Verbanac et al., 2011) the intensity being mainly dependent on the orientation of the IMF and the dynamic pressure of the solar wind.

Following solar maximum, the coronal holes which are prevalent at the poles begin to extend towards equatorial latitudes, sometimes crossing the helio-equator. At solar minimum the high-speed wind dominates at high latitudes, while the low-speed component coexists at lower latitudes with occasional high-speed streams. Low-latitude coronal holes are therefore most evident during the declining years of sunspot activity following solar maximum and before solar minimum.

A typical fast solar wind stream from a low-latitude coronal hole has a compression region (or co-rotating interaction region (Heber et al., 1999) on the leading edge (which may have an associated shock front) and a rarefaction region on the trailing edge. In terms of geospace effects, the co-rotating interaction region is the dominant component of a fast solar wind stream, though the strength and duration of the southward component of the interplanetary magnetic field, the strength of the solar wind pressure pulse, and the prior state of the magnetosphere are also significant factors affecting geo-effectiveness (Hajra and Sunny, 2022).

In 2005, as solar activity declined towards minimum, the solar wind was dominated by fast streams emanating from recurrent equatorial coronal holes. The solar particle event under consideration occurred during this period and resulted from the heliomeridional passage across the solar disc by a coronal hole (Figure 1) which induced a moderate geomagnetic storm during July 1 and 2. This was the largest equatorial coronal hole to emerge since the 'Elephant's Trunk' of summer 1996 (Del Zanna and Bromage, 1999).

This study uses data from the ACE (McComas et al., 1998; Smith et al., 1998) and Wind (Ogilvie et al., 1995; Lepping et al., 1995) spacecraft, both located in the vicinity of the L1

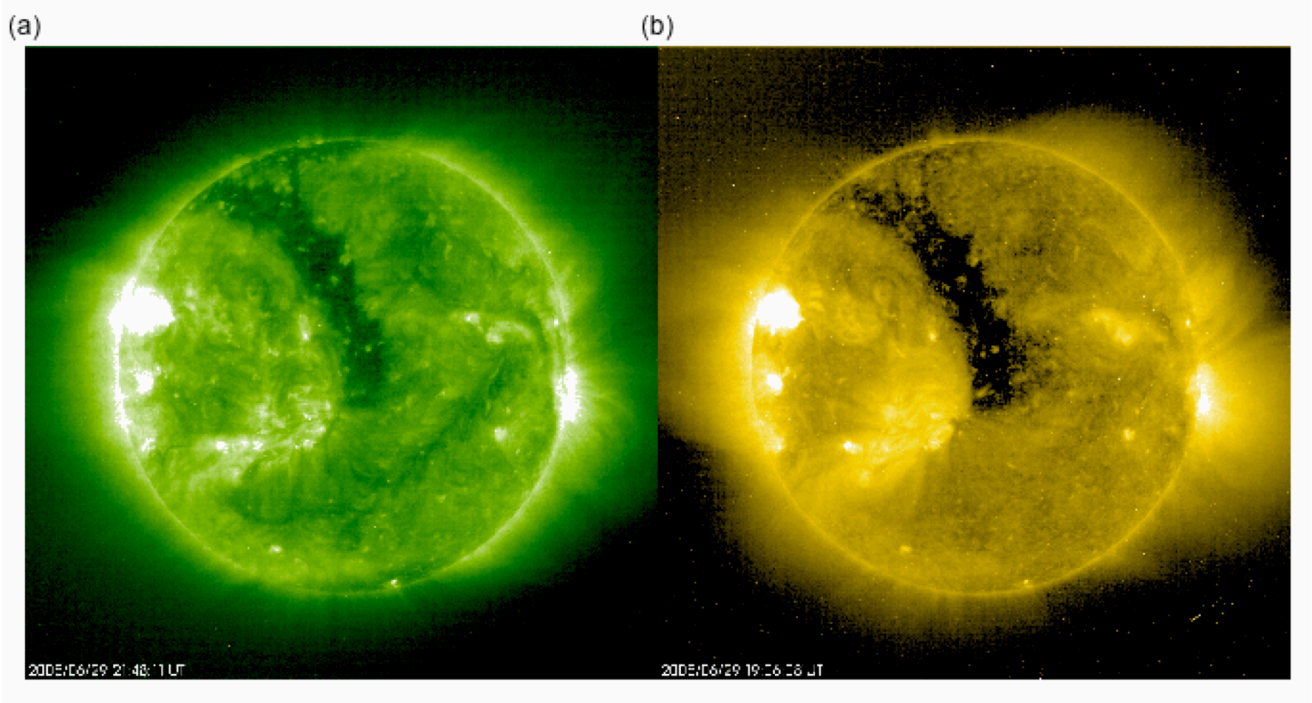

Figure 1: Images of the Sun from the EIT instrument aboard the SOHO spacecraft at L1, June 29, 2005: (a) 195$\mathring{A}$ at 21:48 UT; (b) 284$\mathring{A}$ at 19:06 UT.

libration point. (Though tasked to study the magnetosphere and the Lunar environment during the first phase of its mission, Wind has been continually in the vicinity of L1 since 2004.) During the period of observation, Wind and ACE were positioned slightly above the ecliptic, on either side of the Sun-Earth line in the XY GSE plane. The configuration is shown in relation to Earth and L1 in Figure 2, and in more detail with respect to L1 in Figure 3.

In this paper an algebraic method is described whereby the velocity of the particle flux of the fast solar wind stream can be determined by measuring the interplanetary magnetic field at the Wind and ACE spacecraft, without recourse to a particle detector. A detailed error analysis is provided, and the application of the method to other spacecraft geometries is discussed.

2 Description of the event at L1.

The leading edge of the coronal hole (Figure 1) first crossed the helio-meridian on June 29 2005 at about 00:00 UT (± 3 hours, the edge being somewhat difficult to discern precisely). The ACE real-time summary plot gives an overview of the complete event over about 6 days (Figure 4). Before the event, quiescent conditions prevailed, typical of the slow solar wind: the density varied from 1 to 3 cm^{-3} (panel 'c'), the speed was steady at ≈400 km/s (panel 'd'), and B_z was limited to oscillations within ≈ ±5 nT (red plot, panel 'a') .

The first clear evidence for the arrival of the co-rotating interaction region can be seen on July 1 at about 13:20 UT: an abrupt increase in density to ≈30 cm^{-3}, the start of a gradual increase in speed, an enhancement in B_t, and strong oscillations in B_z. (Though there is a brief data gap in ACE density at the arrival time of the compression region, the velocity data (not

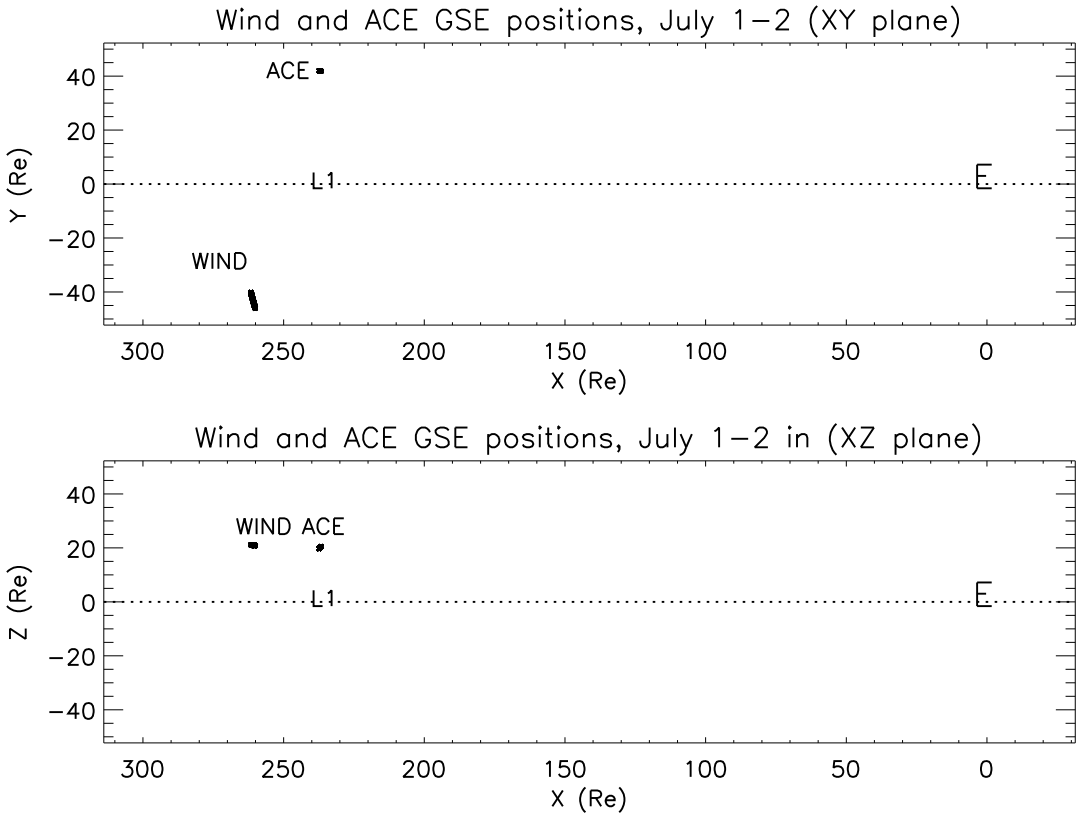

Figure 2: The geometry of Wind and ACE in the vicinity of Earth (E) and L1 during the event.

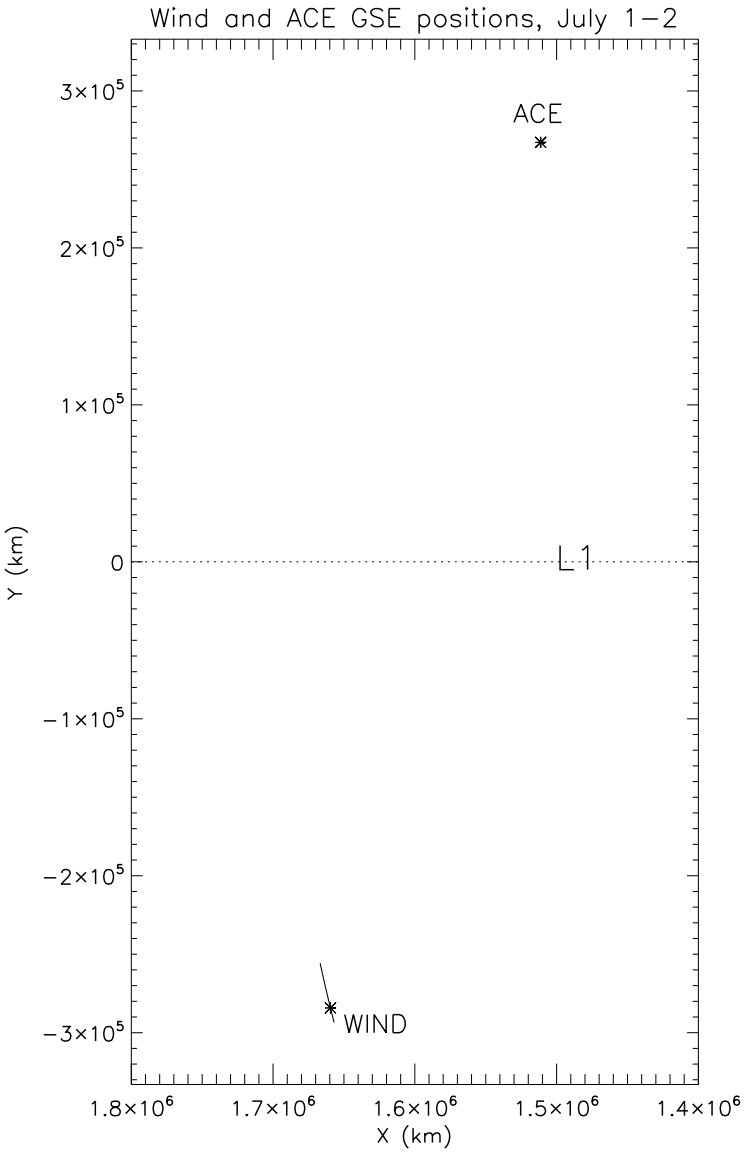

Figure 3: The detailed geometry of Wind and ACE in the vicinity of L1 during the event (the mean separation in X is 151200 km).

shown) gives an estimate of 13:20 UT.)

The interval of maximum activity lasted from 13:20 UT on July 1 to about 06:00 UT on July 2: strong oscillations in B_z (with southerly excursions to ≈-12 nT at 15:30, 17:30 and 21:30 UT, each of duration 1 to 2 hours); an enhancement in B_t to ≈ 18 nT; an abrupt increase in speed to ≈650 km/s; and a gradual reduction in density to ≈5 cm^{-3}.

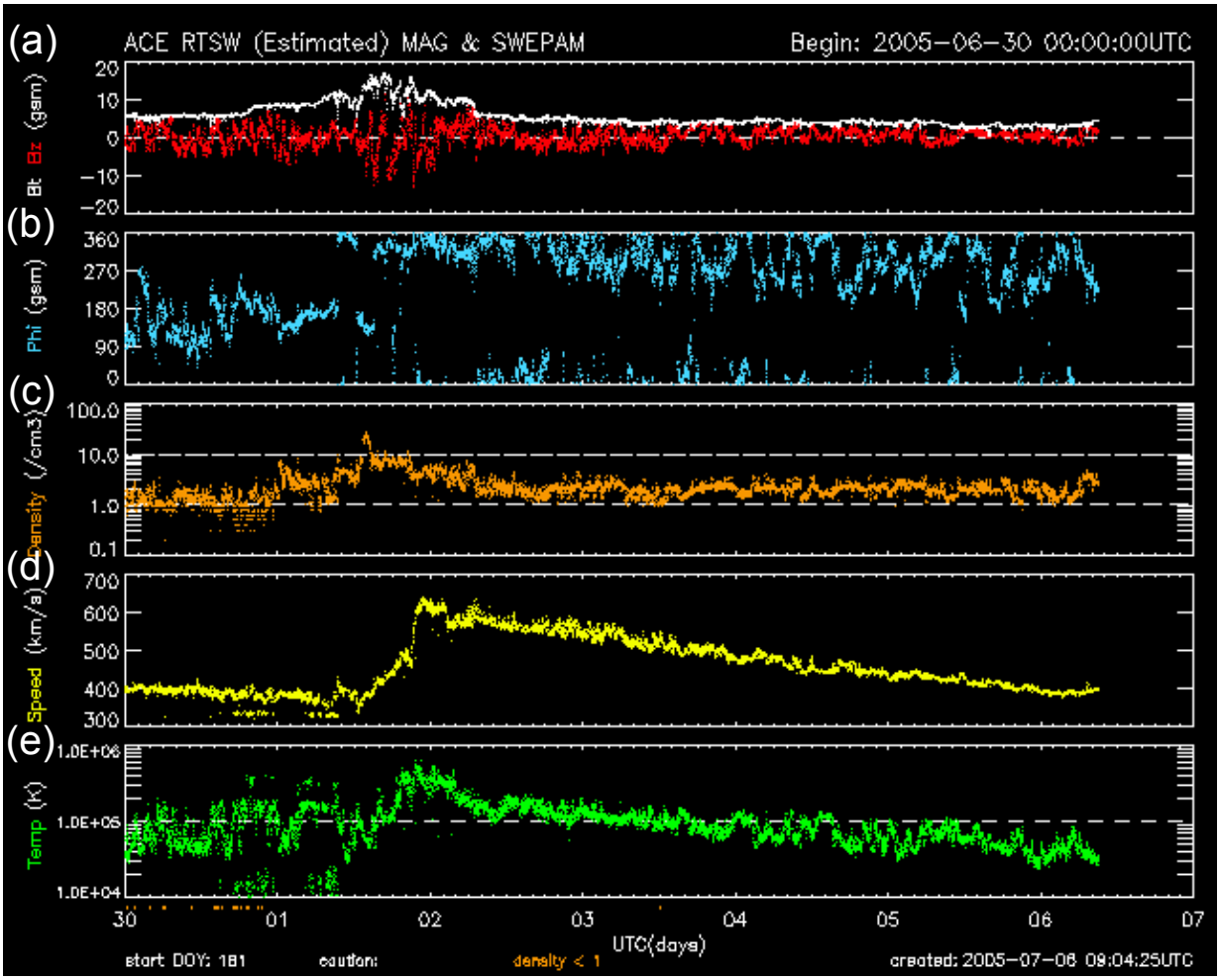

Figure 4: Real-time ACE plots of the solar wind environment at the L1 libration point from June 30 to July 6 2005: (red) IMF B_z (nT); (white) IMF B_t (nT); (blue) IMF clock angle (degrees); (orange) solar wind density (/cm^3); (yellow) solar wind speed (km/s); (green) solar wind temperature (°K). (Courtesy of the ACE Science Centre, California Institute of Technology.)

After 06:00 UT on July 2, over a recovery period which lasted more than 4 days, the solar wind gradually returned to behaviour characteristic of the slow component: the speed decreased gradually to about 400 km.s^{-1}, and B_z, B_t and density returned to their pre-event levels.

Figure 5 shows in greater detail the variations in B_z, P_{dyn} and solar wind speed at the Wind spacecraft from 00:00 UT on July 1 to 12:00 UT on July 2, the most active period. Of

particular interest is the abrupt increase in dynamic pressure (panel 'b') at 13:00 UT (dashed line) resulting from the order of magnitude increase in density at that time. It is likely that this dynamic pressure pulse caused the weak sudden commencement recorded at 14:12 UT (Figure 6) by the ground-based magnetometers at Shigaraki (34.8° N, 136.1° W), Urumqi (43.8° N, 87.7° W), and Kakioka (36.2° N, 140.2° W). The 'dash-dot' line in Figure 5 indicates the approximate end of the magnetic 'packet' characteristic of the compression region (the significance of the dotted lines will be covered in Section 4).

During the interval from 15:00 UT on July 1st to 03:00 UT on July 2nd the average K_p index increased to 4, indicating moderate storm conditions. Throughout this interval solar wind density, speed and temperature were markedly enhanced, and B_z showed its strongest southerly oscillations.

This was a particularly 'clean' event; no other significant geoeffective solar activity from X-ray flares or CMEs was observed throughout the period of fast solar wind resulting from the meridian passage of the coronal hole. This lack of transient activity, and the gradual 'arch' shape of the coronal hole as it extends northwards from the helio-equator, probably explain the remarkably linear decline in solar wind speed during the recovery phase of the event.

3 Delays in the IMF between Wind and ACE using selected features

The average solar wind speed from the Sun to the Earth can be estimated by dividing the total distance (1.52e+08 km) by the difference between the time at which the leading edge of the coronal hole first crossed the helio-meridian (00:00 UT on June 29th) and the time at which the sudden commencement occurred (14:12 UT on July 1st). This gives 679±32 km.s^{-1}, the main uncertainty being in the estimate of the helio-meridian crossing (±3 hours).

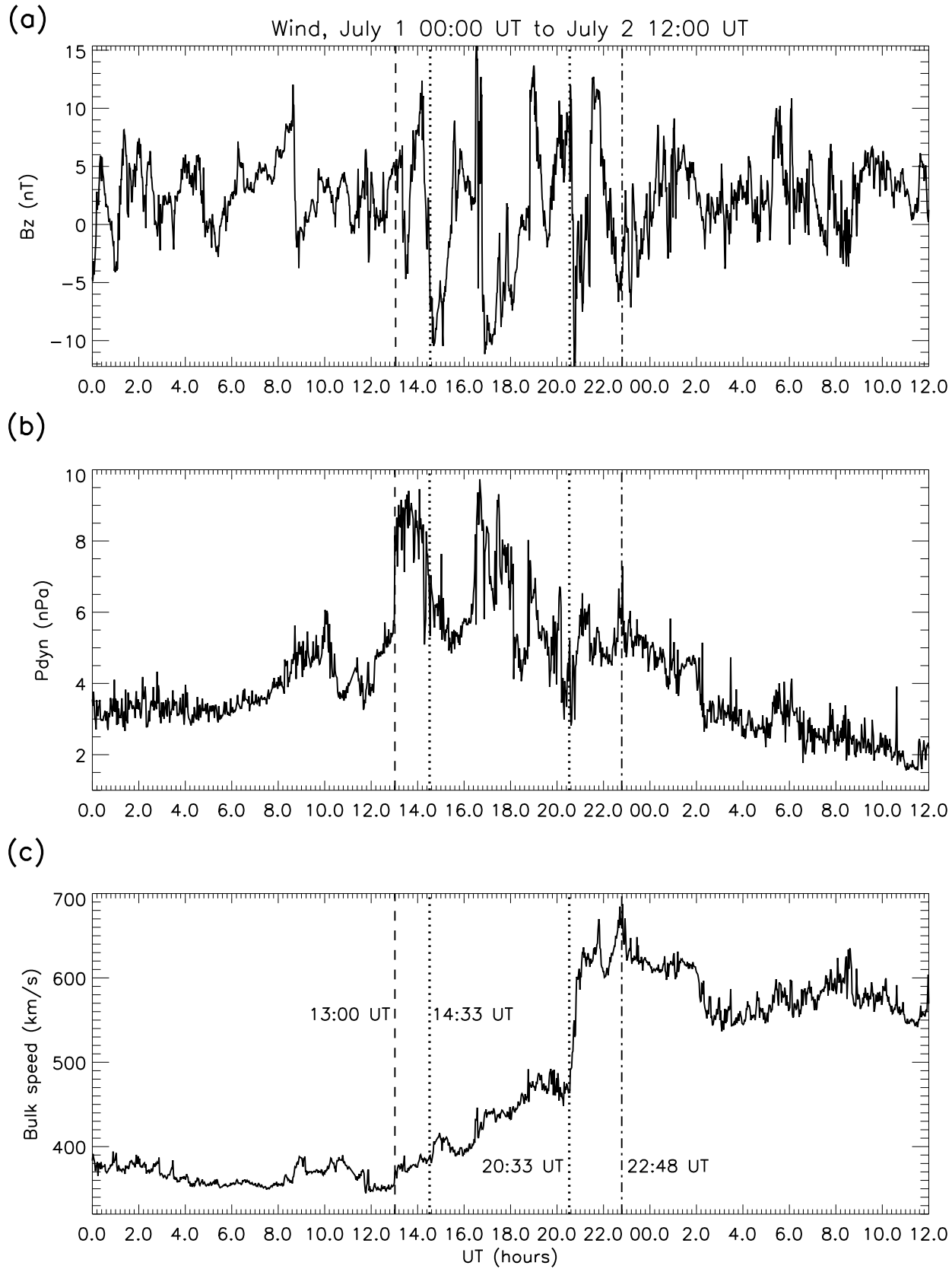

Figure 5: Wind observations from 00:00 UT on July 1 to 12:00 UT on July 2 (1 min. data): (a) IMF B_z (nT); (b) SW dynamic pressure (nPa); (c) SW bulk speed (km/s). (The dashed line marks the start of the event, the dotted lines mark the interval of optimum correlation of B_z, and the dot-dash line marks the approximate end of the event.)

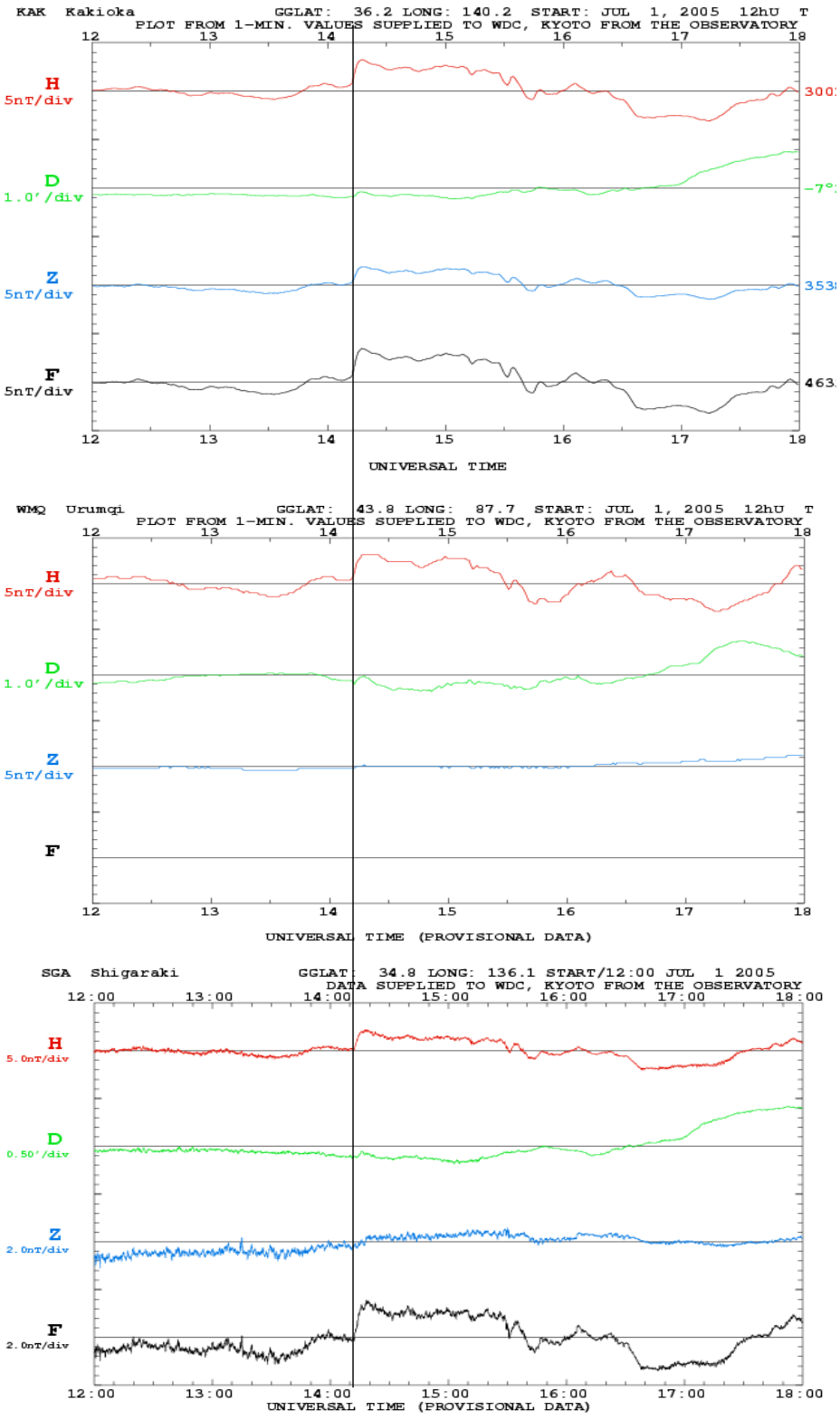

Figure 6: Magnetometer responses to the arrival of the co-rotating interaction region at the magnetopause on July 1st, at Kakioka, Urumqi and Shigaraki. The vertical line marks the sudden commencement at 14:12 UT.

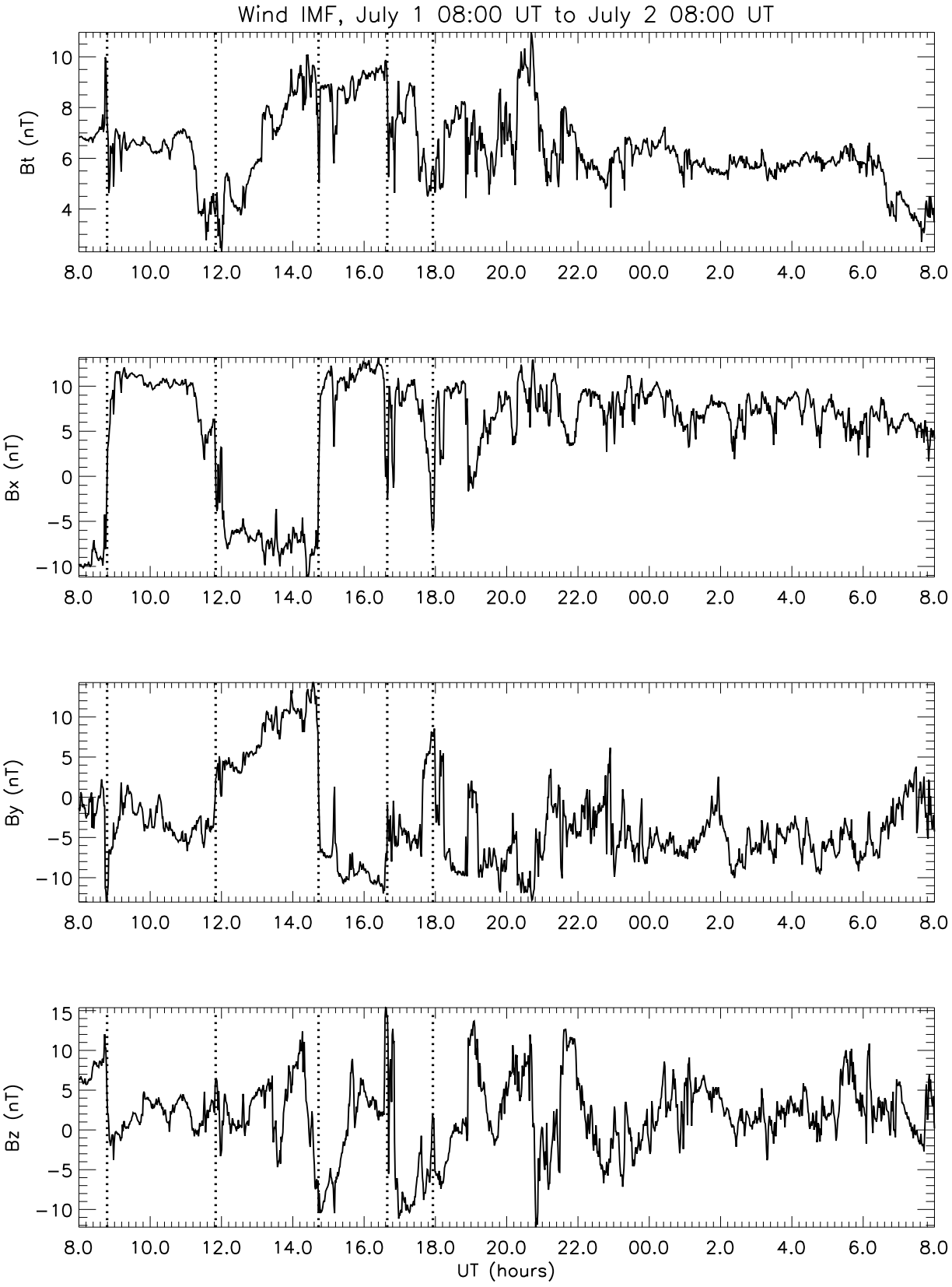

Figure 7: IMF flux density at the Wind spacecraft during July 1st and July 2nd, 2005. (The dotted lines mark the features selected for comparison with ACE in Figure 8.)

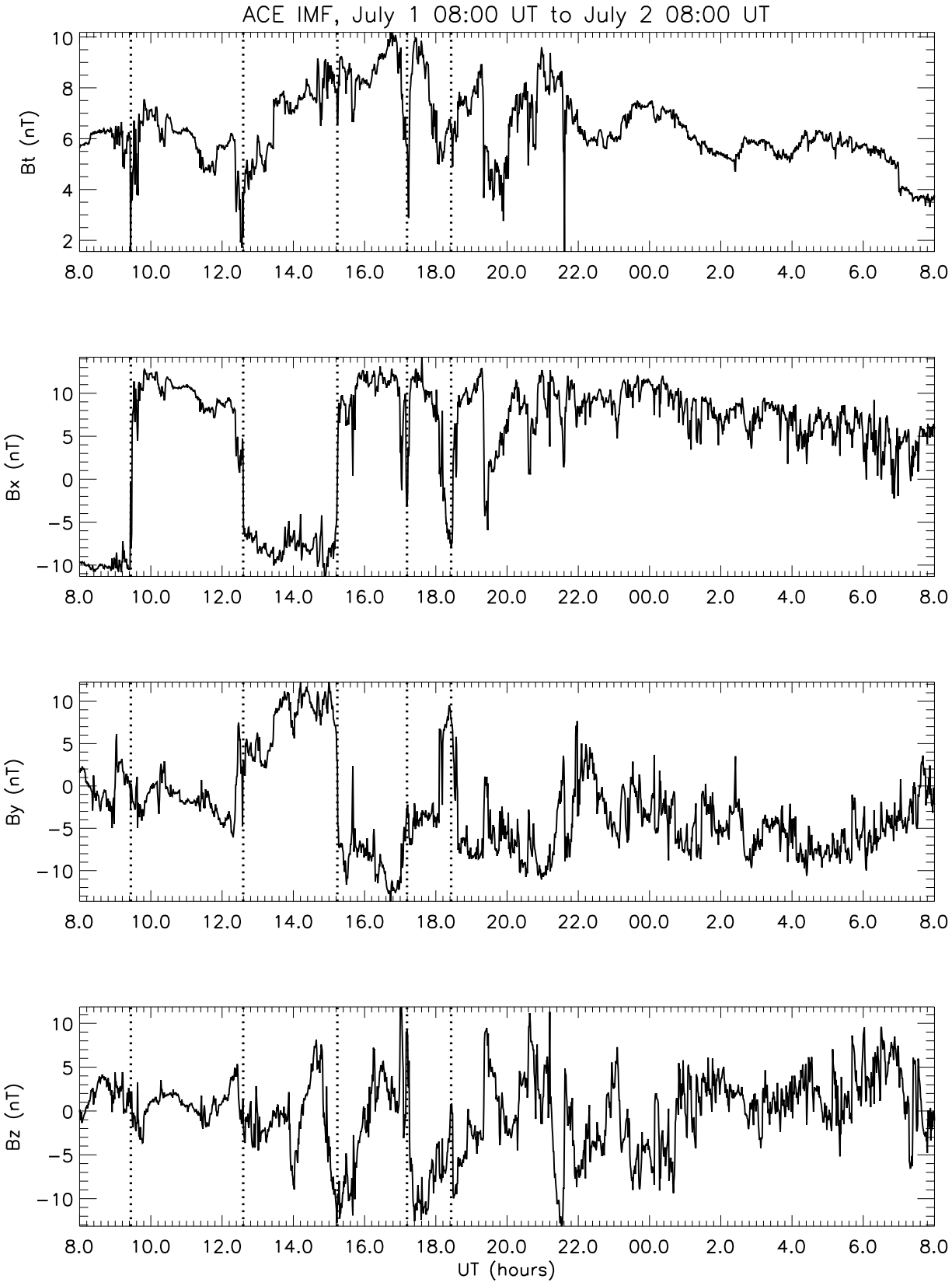

Figure 8: IMF flux density at the ACE spacecraft during July 1st and July 2nd, 2005. (The dotted lines mark the features selected for comparison with Wind in Figure 7.)

Alternatively, the average speed can be estimated by dividing the distance from the Sun to L1 by the difference between the time of the helio-meridian crossing (the same as above) and the time that the event was first detected at L1 (by using the leading edge of the dynamic pressure pulse, at about 13:00 UT at Wind). This method gives a velocity of 685±32 km.s^{-1}, the time of the helio-meridian crossing once again being the dominant uncertainty in this estimate. However, these estimates give only the average speed over the total distance from the Sun, and we require the speed at L1, without recourse to a particle detector.

The IMF measurements from both Wind and ACE are clearly similar for this event (Figures 7 and 8). (As will subsequently be seen, it is the coherent nature of the two independent time series of N/S magnetic flux density (B_z) which enables the determination of the solar wind speed.) Using for comparison five clearly identifiable features in the IMF (three sector boundary changes in B_x and B_y, and two significant spikes in B_z), five delay times were measured: (ACE, Wind) = (9.36, 8.71), (12.51, 11.76), (15.16, 14.64), (17.11, 16.57) and (18.35, 17.85) hours. These measurements (taken from 1-minute data files) give delays of 39, 45, 31, 32, and 30 minutes, giving a mean of 35 minutes with a standard deviation of 6 minutes.

Clearly, the delays derived from these spot values vary considerably and are not reliable measures. Consequently, a running cross-correlation was performed on the Wind and ACE IMF data in order to determine a delay free from the variations necessarily associated with point-to-point selections.

4 Correlation of B_z at Wind and ACE during the event

Wind and ACE 1-second B_z time series were used in these correlation tests (the analysis soon revealed that B_t, B_x, and B_y gave very poor results). A lagged cross-correlation of the ACE and Wind time series covering the entire event would not have been suitable for determining

the delay because the limits of the event and the centre of activity are not defined, and so the result cannot be compared with a measured solar wind speed. Instead, a series of 11 running cross-correlations were carried out on the Wind B_z data from 06:00 UT on July 1 to 06:00 UT on July 2, against successively increasing intervals in ACE B_z data, each centred at 18:00 UT on July 1, and each of duration $\pm n$ hours, where $n = 1.0...6.0$ in 0.5 hour increments. (Tests with ACE B_z centred from 14:00 to 22:00 UT in 1-hour increments showed a rapid reduction in correlation when the centre diverged from 18:00 UT, proving this to be the mid-point of the IMF activity.)

In the resulting correlograms, as n increases, a distinct peak in the correlation coefficient (ρ) steadily emerges above the background. However, the value of ρ associated with each peak does not increase with n, as can be seen in Figure 9a. In fact, there is a distinct peak for $n = 1.5$, 2.0, 2.5 and 3.0 ($\rho = 0.90$, 0.88, 0.87, and 0.88, respectively), all of which give a delay of 1610 seconds (Figure 9b), with Wind preceding ACE.

The correlograms for each of these four values of n are shown in Figure 10, in which the peak emerges above the background as the width of the ACE interval increases from $n = 1.5$ to $n = 3.0$. It is considered that the ACE interval defined by $n = 3$ (from 15:00 to 21:00 UT), with $\rho = 0.88$, gives the optimum correlation (the peak is more distinct relative to the background, even though $\rho = 0.90$ when $n = 1.5$). The result is clearly robust, because all four values of n give the same delay which, when applied to Wind, gives the optimum interval from 14:33 to 20:33 UT (27 minutes delay, to the nearest minute). These UT limits are marked in Figure 5c as dotted lines.

With a mean separation between Wind and ACE of 149820 km, this 1610-second delay gives a mean solar wind speed of 93.4 km/s, which is obviously incorrect, being based on a delay in the *field*, not the *particles*. Consequently, consideration must now be given to the relationship

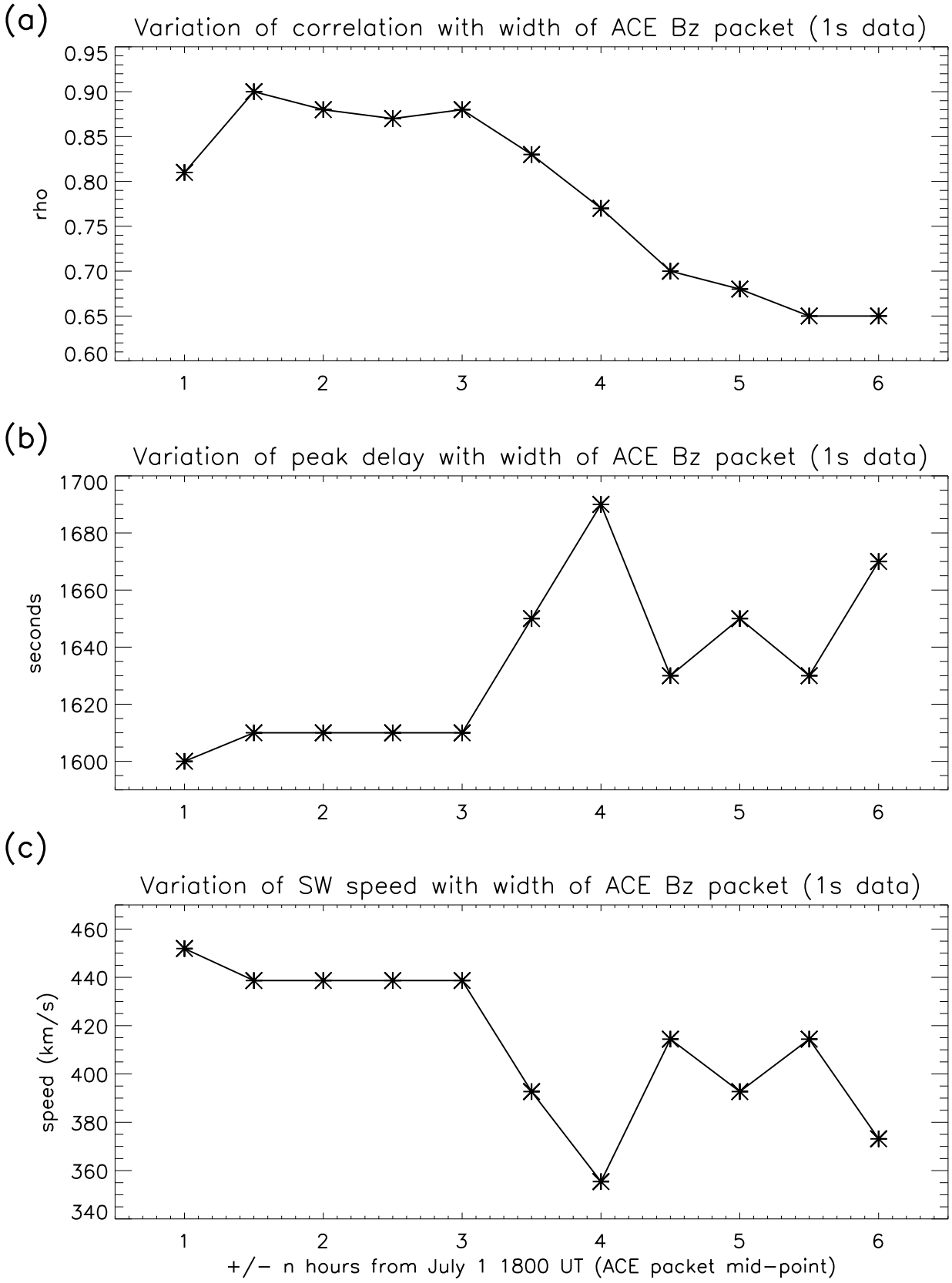

Figure 9: Correlation of Wind B_z against the ACE B_z (1 s data), relative to width of ACE interval: (a) correlation coefficient; (b) peak delay; (c) solar wind speed (deduced from the delay, using the algebraic model).

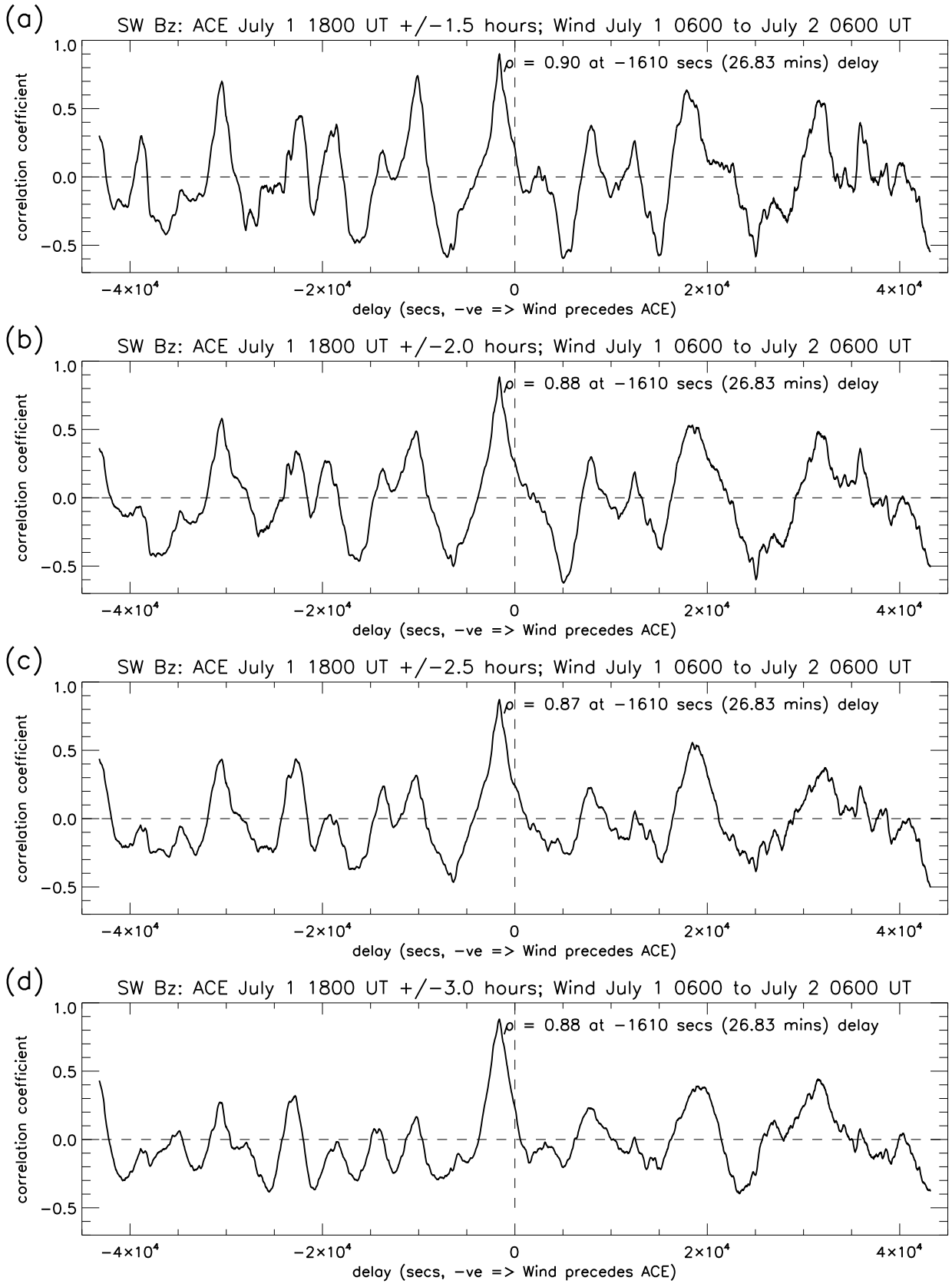

Figure 10: Correlograms of 1-second B_z time series for ACE (on July 1 at 18:00 UT $\pm$ n hours) against Wind (from 06:00 UT on July 1 to 06:00 UT on July 2): (a) $n = 1.5$ hours; (b) $n = 2.0$ hours; (c) $n = 2.5$ hours; (d) $n = 3.0$ hours.

between the solar wind and its embedded magnetic field.

5 An algebraic model of the field line geometry at L1.

The solar wind speed cannot simply be derived by dividing the separation of Wind and ACE along the Sun-Earth axis by the delay in the field, because the particles emanate radially from the Sun as it rotates, but the frozen-in magnetic field is rooted at the photosphere. Any given field line represents the locus of all the particles originating at a single location on the solar surface, forming an Archimedean (or Parker) spiral (Parker, 1958), a curve which in polar coordinates (r, θ) can be described by the equation $r = a + b\theta$. For the solar wind, a represents the solar rotation rate and b the bulk speed (effectively, the speed in the Sun-Earth direction). For example, $b = 250$ (km/s) gives a typical field line with the angle between the spiral and the Sun-Earth line at 1 AU being $\approx 45°$, which is indeed the angle confirmed by observation during periods when this solar wind speed is dominant.

By demonstrating how the process of field line growth in the vicinity of L1 is related to the particle flux it is possible to calculate algebraically the speed of the fast solar wind stream as a function of the delay in the IMF between two spacecraft at known locations, without recourse to a numerical computation of field line growth (which is very demanding in terms of computing time).

The Sun-Wind-ACE IMF system is shown schematically in Figure 11. A single location (i.e a single field line) is considered. An element of solar wind plasma is emitted from solar location S_w, travels radially along the Sun-Wind line and subsequently arrives at the Wind spacecraft (P_w), carrying with it the magnetic signature of its source location at the solar surface. During the travel time of the plasma element to P_w, the Sun has rotated for time period ΔT_s ($= \Delta T_w + \Delta T_a$), and released a further element from the same solar location (now at position S_a) which

has travelled radially along the Sun-ACE line to position P_a.

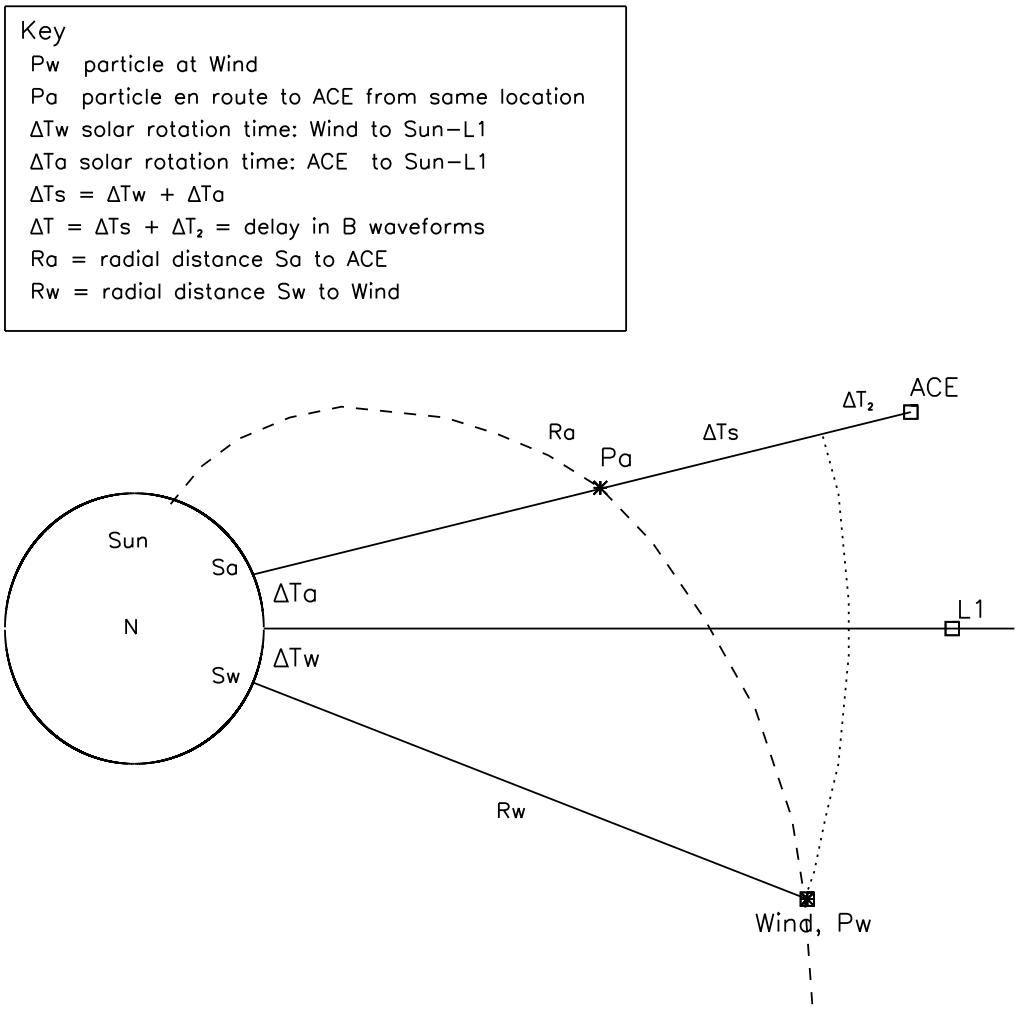

Figure 11: Geometry of Sun, ACE and Wind, showing particles emitted radially from a single location on the solar surface (and which therefore occupy the same field line).

$$\Delta T_s = \Delta T_w + \Delta T_a \tag{1}$$

It is assumed: (i) that the magnetic field strength of the solar plasma at the location considered does not significantly change during the rotation from S_w to S_a, and (ii) that the plasma is emitted at the same speed from both locations. These assumptions are considered to be reasonable because the rotation time ΔT_s is only 1268 seconds. (Of course, though plasma is

emitted continuously, only those elements relevant to this model are considered.)

The total (correlated) delay in the field (ΔT) between Wind and ACE consists of two components: (i) the delay resulting from solar rotation ($\Delta \mathrm{T}_s$), and (ii) that resulting from the difference in the radial distances of Wind and ACE from the Sun ($\Delta \mathrm{T}_2$) -

$$\Delta T = \Delta T_s + \Delta T_2 \tag{2}$$

The solar wind travels the difference in the radial distances between Wind (R_w) and ACE (R_a) at speed V_x in time $\Delta \mathrm{T}_2$ -

$$\Delta T_2 = \frac{R_a - R_w}{V_x} \tag{3}$$

Eliminating $\Delta \mathrm{T}_2$, these three equations reduce to the relation -

$$V_x = \frac{R_a - R_w}{\Delta T - \Delta T_s}, \tag{4}$$

or

$$V_x = \frac{\Delta R}{\Delta T - \Delta T_s}. \tag{5}$$

Consequently, the solar wind speed is given by the ratio of the difference in the distances of Wind and ACE from the Sun to the difference between the correlated delay in the IMF from Wind to ACE and the solar rotation time between the Wind and ACE sub-solar locations.

In developing this algebraic model, the only assumptions made about the nature of the solar wind are that, over large distances (such as from the Sun to L1): (i) on average, particles in the heliosphere travel in straight radial lines, and (ii) over short time intervals (typically, minutes) particles from the same location on the Sun travel at the same average speed.

6 Use of the model for the event in question.

[It is emphasised that the Sun-to-Earth distance is 100 times that between L1 and Earth, and about 1000 times the distances in the vicinity of the ACE-Wind-L1 system. Consequently, the angle subtended at Sun-centre by Wind and ACE is only about 0.2°, which justifies the geometric approximations made below.]

In equation 5, the value of ΔT when ACE and Wind exhibit peak correlation in B_z (ΔT_c = 1610 seconds from Section 4) is already known for the event in question, but ΔR and ΔT_s have yet to be determined.

Tests proved that, on these distance scales, the spacecraft are close enough to the Sun-Earth line for the Y and Z components of the spacecraft positions to have a negligible effect on the outcome. Consequently, ΔR (the distance between ACE and Wind along the Sun-Earth line) is equal to the distance between the GSE X components of ACE (at 18:00 UT) and Wind (at 17:33 UT, 27 minutes earlier according to the correlation test) on July 1:

$$\Delta R = |X_w - X_a| \tag{6}$$

ΔT_s (the time taken for the locus of a field line on the Sun to rotate from the Sun-Wind line to the Sun-ACE line) is a function of the angle subtended at Sun-centre by Wind and ACE (θ_{wa}, in radians) and the time taken (T_{sun}) for the Sun to complete one rotation (2π radians):

$$\Delta T_s = T_{sun}.\frac{\theta_{wa}}{2\pi} \tag{7}$$

For T_{sun} we adopt the Carrington sidereal rotation time (25.38 days), based on a helio-latitude of 26°. The variable θ_{wa} (radians) is the ratio of length of the arc of the sector subtended by Wind and ACE at the Sun (Y_{wa}) and the distance from the Sun to the Wind-ACE system

(X_{swa}):

$$\theta_{wa} = \frac{Y_{wa}}{X_{swa}} \tag{8}$$

Assuming that it is not an arc but a straight line (reasonable on these scales), Y_{wa} is the sum of the GSE Y components of ACE and Wind:

$$Y_{wa} = Y_w + Y_a \tag{9}$$

X_{swa}, the mean distance between the Sun and the Wind-ACE system, is the difference between the Sun-Earth distance (X_{se}) and the distance of the Wind-ACE system from Earth:

$$X_{swa} = X_{se} - X_{wa} \tag{10}$$

The distance of the Wind-ACE system from Earth is assumed to be equal to the mean distance of Wind and ACE from Earth (because $X_{wa} << X_{se}$):

$$X_{wa} = \frac{X_w + X_a}{2} \tag{11}$$

Finally, X_{se} is the Sun-Earth distance, which is the product of the mean value for 1 AU (1.495978707 x 10^8 km) and a correction factor (1.016701) based on the fact that Earth's orbit has an eccentricity of 0.0167 (http://www.astropixels.com/ephemeris/perap2001.html).

Inserting equations 8 to 11 into equation 7 gives:

$$\Delta T_s = \frac{T_{sun}(Y_w + Y_a)}{\pi(2X_{se} - X_w - X_a)} \tag{12}$$

Equations 5, 6 and 12 can then be reduced to a single formula which derives the solar wind speed at the time of peak correlation (V_c) from a set of fundamental parameters (the values of

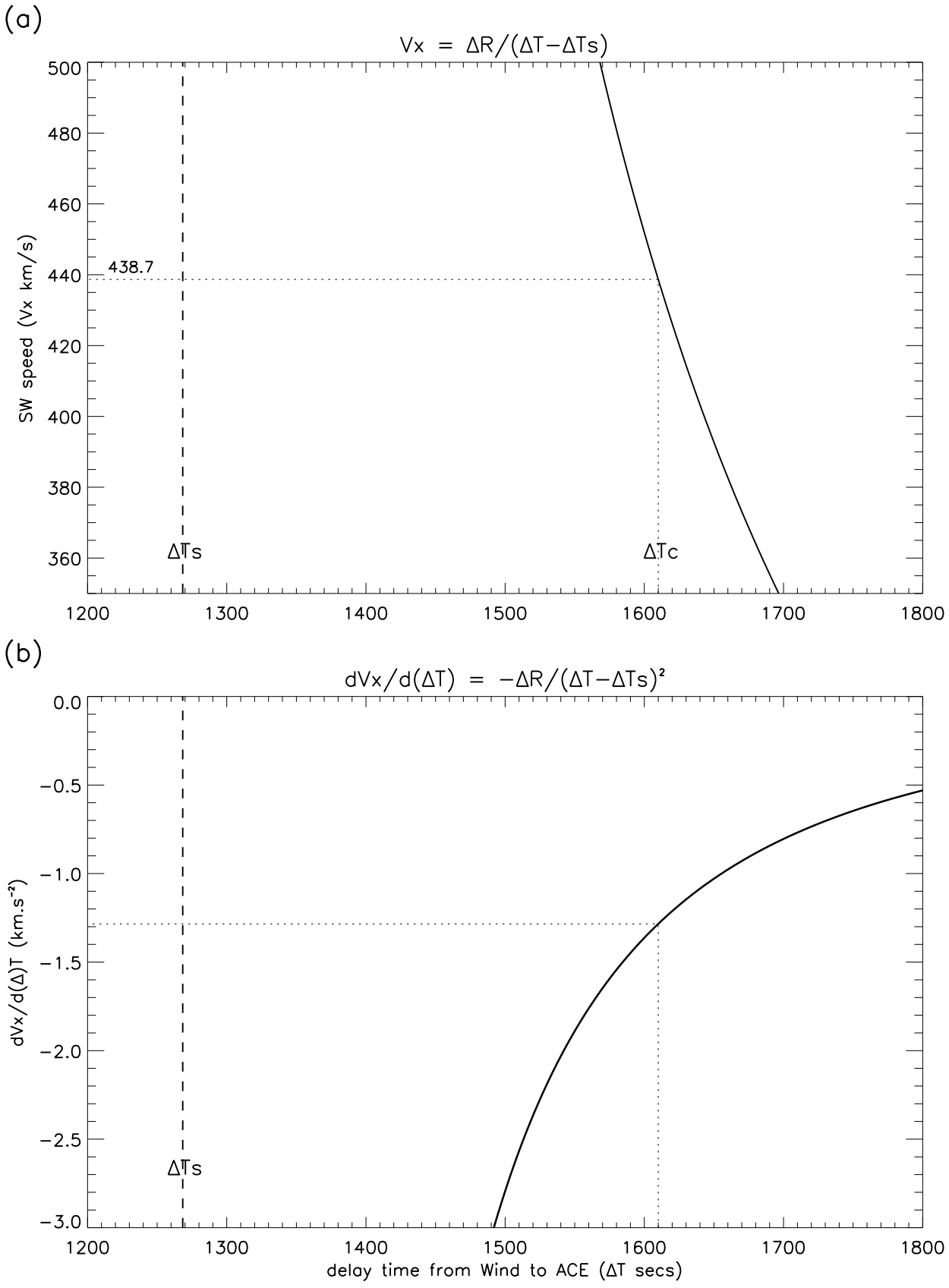

Figure 12: (a) Results of the algebraic model for the parameter values in Table 1. (b) Derivative, $dV_x/d(\Delta T)$. (Error bars are too small to be discernible on these plots.)

	Parameter	Symbol	Value	Units	Uncertainty
1	Wind-ACE B_z delay time	ΔT_c	1610	secs	negligible
2	Sun-Earth distance	X_{se}	$1.51993.10^8$	km	negligible
3	Solar sidereal rotation period (Carrington)	T_{sun}	25.38	days	± 0.01
4	ACE GSE x component	X_a	1510923	km	± 40
5	ACE GSE y component	Y_a	266957	km	± 40
6	Wind GSE x component	X_w	1660791	km	± 20
7	Wind GSE y component	Y_w	279663	km	± 20

Table 1: Fundamental parameters required by equation 13

which are listed in Table 1):

$$V_c = \frac{\pi(X_w - X_a)(2X_{se} - X_w - X_a)}{\pi\Delta T_c(2X_{se} - X_w - X_a) - T_{sun}(Y_a + Y_w)} \tag{13}$$

Substituting the values in Table 1 into equation 12 gives a solar wind speed of 438.7 km/s (Figure 12a), a value which agrees very closely with the speed measured by Wind at 17:33 UT on July 1 (436.6 km/s), and that measured by ACE at 18:00 UT (437.3). This speed is near the boundary between the slow and fast solar wind (400 - 450 km/s).

7 Discussion

7.1 Error analysis

The total error in V_x is a function of the individual errors in the fundamental parameters listed in Table 1. As regards the error in ΔT_c (parameter 1), correlation tests between the Wind and ACE 1-second B_z data revealed that a distinct delay (1610 seconds) can be derived from the period of maximum activity (centred at 18:00 UT on July 1) in which B_z is most structured.

The correlation coefficient remains almost constant (0.87 to 0.90) when the duration of this period varies from 3 to 6 (± 1.5 to 3.0) hours. This is considered to be a robust result for which the delay can be assumed to be accurate to within 1 second. As the derivative of V_x shows (Figure 12b), $dV_x/d(\Delta T)$ is only -1.28 km.s^{-2}, which means that V_x is accurate to within ±1 km.s^{-1}.

However, the errors in ΔR and ΔT_s must also be taken into account, which are dependent on parameters 2 to 7 in Table 1. The Sun-Earth distance (X_{se}) has been corrected for Earth's orbit eccentricity on July 1 2005 by interpolation of a table of aphelion and perihelion values (the aphelion being on July 5), so the error is assumed to be negligible. The Carrington sidereal solar rotation time (T_{sun}), consistent with the latitude of periodic solar activity, is a well-known parameter which has an uncertainty of no more than ±0.01 days (209 seconds). This also gives an accuracy for V_x to within ±1 km.s^{-1}. The errors in the X and Y GSE positions of Wind and ACE, provided by NASA GSFC, are within ±20 and 40 km (respectively). Tests show that the effect of this uncertainty is negligible.

To summarise, the combined effect of the errors in Table 1 is that, using this method, the deduced solar wind speed is accurate to within ±1 km.s^{-1} overall. When plotted, this value is too small to discern in Figure 12.

7.2 Limits of applicability.

To assess the efficacy of this method for other spacecraft geometries it is necessary to consider their proximity in relation to the response of equation 5 when ΔT_s and ΔR vary, and to consider how these variations affect not only the function itself, but also the gradient $dV_x/d(\Delta T)$ (which determines the sensitivity of V_x with respect to ΔT). It is the gradient that is the significant factor in this discussion.

Varying ΔT_s (the angular separation of the spacecraft at Sun-centre) only translates the curve and its asymptote on the abscissa in Figure 12. This will have no effect on the accuracy of the deduced speed with respect to ΔT. Consequently, there are no limits on the angular separation of the two spacecraft, except for the reduction in waveform coherence which is in turn affected by event intensity (discussed below).

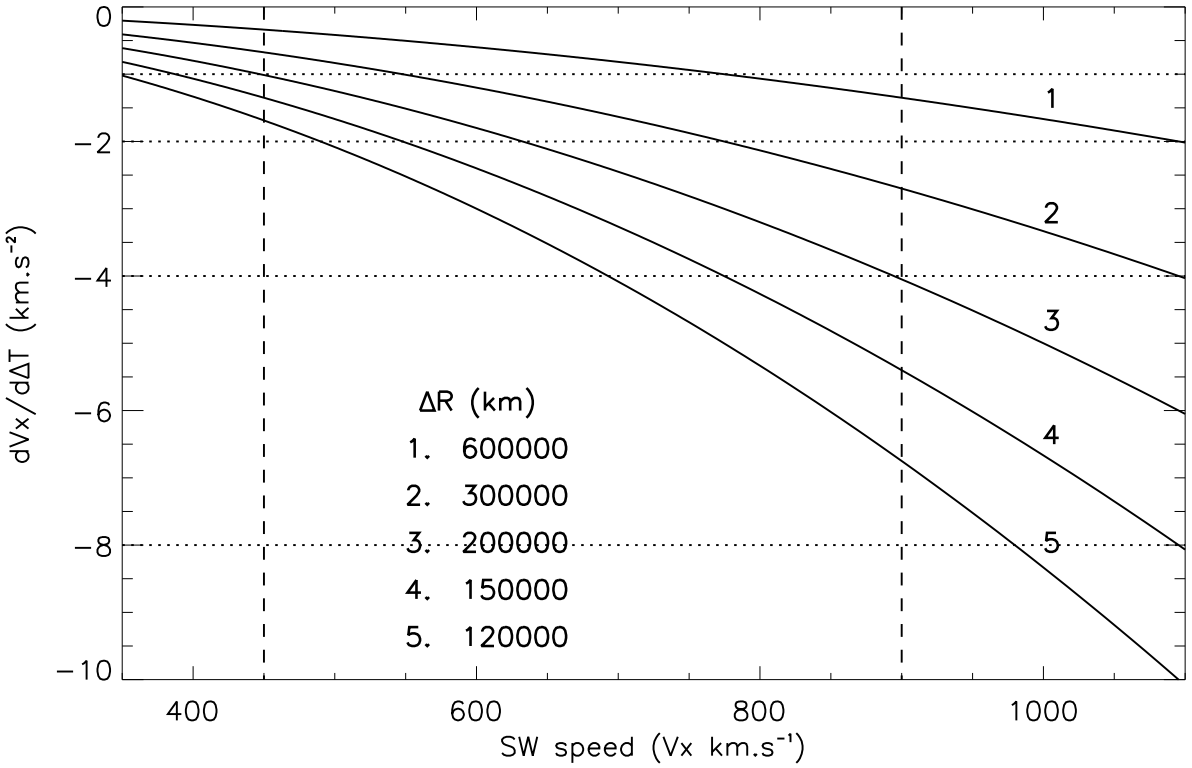

Figure 13: Variation of $dV_x/d(\Delta T)$ with V_x (ΔR increasing from 120000 to 600000 km, and ΔT_s fixed at 1268 s). The dashed lines mark the nominal limits of the fast solar wind.

The effect of ΔR on the accuracy of the deduced speed is more significant. Figure 13 shows how $dV_x/d(\Delta T)$ varies with speed, for a range of values of ΔR from 120000 to 600000 km. The approximate limits of the fast solar wind (450-900 km.s^{-1}) are marked by dashed lines, and the gradient values at -1, -2, -4 and -8 km.s^{-2} are marked by dotted lines. The variation in the accuracy of the deduced speed over a range of values of ΔR can now be investigated.

If an accuracy of 1 km.s^{-1} is required, then at a separation of 600000 km (curve 1 in Figure 13) the maximum speed that can be deduced is 770 km.s^{-1} (though for slower speeds even higher accuracy is attainable). At half the separation (curve 2) only speeds up to 550 km.s^{-1} can be deduced to 1 km.s^{-1} accuracy. As the separation decreases, this trend continues, so that in the case of curve 5 (separation 120000 km) the solar wind speed must be as low as 350 km.s^{-1} (which is clearly in the slow domain where IMF structure is lacking and therefore sufficient correlation is unlikely). For a lower accuracy the speed constraint can be relaxed. For example, if 4 km.s^{-1} is acceptable, then curve 3 shows that a maximum solar wind speed of 900 km.s^{-1} can be deduced at a separation of 200000 km, higher speeds requiring greater separation (though speeds rarely exceed 1000 km.s^{-1}).

The implications of Figure 13 are summarised in Table 2. This shows that, for the highest accuracy (1.0 km.s^{-2}), a separation of over 600000 km is required to cover fast solar wind speeds up to 770 km.s^{-1}. However, if the accuracy constraint is relaxed to 8.0 km.s^{-2} the full range of fast solar wind speeds can be accommodated at a separation as low as 120000 km.

Accuracy in deduced V_x for $\Delta T = \pm 1$s ($\pm$km.s^{-1})	Maximum solar wind speed (km.s^{-1}) for spacecraft separation (ΔR km)				
	120000	150000	200000	300000	600000
1.0	350	380	450	550	770
2.0	490	550	640	770	1100
4.0	690	770	900	1100	>1100
8.0	975	1100	>1100	>1100	>1100

Table 2: Maximum solar wind speed that can be deduced in equation 5, for variations in accuracy and spacecraft separation (from Figure 13.

There is, however, another important factor: the coherence of B_z will diminish with increasing spacecraft separation, reducing the correlation coefficient, and therefore the accuracy of ΔT_c. Richardson and Paularena (2001) used IMF data from multiple spacecraft to determine IMF correlation coefficients for more than 4000 6-hour periods from 1997 to 1998 (irrespective of solar wind speed). As X separations increased from 0 to 280 R_e (1.78 x 10^6 km) the correlation coefficients decreased by $\leq$0.1. There was much more variation of the correlation coefficients with spacecraft separation in the YZ plane, with a significant decrease for separations greater than 45 R_e (2.87 x 10^5 km).

Weygand et al (2011) used simultaneous multi-point measurements of the IMF from 11 spacecraft to determine the correlation scale of the solar wind as a function of the mean magnetic field direction and solar wind speed, involving a total of about 4400 cross-correlations. At speeds $\leq$600 km.s^{-1} the correlation coefficient decreased from 1.0 (at zero separation) to 0.4 in the X direction and 0.2 in the YZ plane (at 2.0 x 10^6 km separation). At speeds >600 km.s^{-1}, the correlation coefficient decreased to 0.2 in the X direction (the YZ value being the same).

These results suggest that there is likely to be a separation limit in both the X and YZ directions beyond which the coherence of B_z reduces to such an extent that the correlation is too weak for equation 5 to give a useful result. However, this limit is difficult to specify because it will also be dependent on the amount of structure present in the IMF, which will in turn be dependent on the intensity of the event under analysis (related to the solar wind speed). For example, it is likely that an energetic CME would provide sufficient structure to allow for greater separations than those herein, though this conjecture has yet to be tested.

(To determine the effect of variations in coherence a statistical approach is required involving a range of selected events with varying levels of activity. A study is in progress that will address this subject.)

7.3 Slow solar wind

The same correlation tests carried out on a period of slow solar wind on June 30 centred at 18:00 UT gave poor results: correlation coefficients from 0.33 to 0.55, with peaks barely above background resulting in extreme, random delays (probably because of insufficient coherence). Consequently, it is concluded that this method is unsuitable for use on the slow solar wind.

7.4 Parker spiral fluctuations

The model developed in Section 5 assumes that the solar wind follows a simple Parker spiral structure: fluctuations due to turbulence or electromagnetic instabilities have not been taken into account (Bian et al., 2022). Turbulence refers to a class of phenomena that characteristically occurs in fluids and plasmas when non-linear effects are dominant. Non-linearity creates complexity, involvement of many degrees of freedom and a lack of predictability (Raouafi et al., 2023), making the true form of the Parker spiral intrinsically statistical (Bian and Li., 2021).

Analysis of heliospheric magnetic field observations suggests that the majority of the fluctuations are transverse, varying in the direction normal to the background magnetic field. Such turbulence will cause the field lines to meander across the mean field direction (Laitinen et al., 2023).

Considering that the model assumes the existence of a non-turbulent Parker spiral, the close agreement between the observed and modelled solar wind speeds (< 2 km/s, or 0.4%) is quite remarkable.

7.5 Use of other spacecraft

Though Wind and ACE have been used in this study, any pair of current or future spacecraft that (1) are located in deep space (i.e. not within planetary magnetospheres), (2) comply with

the limits of applicability defined in Section 7.2, and (3) carry onboard magnetometers, can potentially be used to determine the speed of the fast solar wind using the method defined herein. Examples of current missions are Ulysses and STEREO, plus the more recent Parker Solar Probe and Solar Orbiter. However, given that these spacecraft are at various and changing locations within the heliosphere, it is very unlikely that any pair will be sufficiently proximate to satisfy condition 2 (the limits of applicability, Section 7.2). Only Wind and ACE, located in the vicinity of L1, are suitable candidates (though future missions may comply).

8 Summary.

An algebraic model has been presented with which the speed of a fast solar wind stream can be deduced from the interplanetary magnetic field using independent observations of B_z by two spacecraft at different locations. A running cross-correlation using ± 3 hours of B_z data at the mid-point of the active period gave a distinct peak with a correlation coefficient of 0.88 and a delay of 1610 seconds. Substituting the cross-correlated delay into the algebraic model gives a solar wind speed of 438.7 km.s^{-1}, a result which agrees with the measured speed at Wind and ACE to within 0.4%.

Though this result is based on a specific case, the model can, in principle, be applied to any two spacecraft that comply with the following conditions -

1. The smaller the radial separation of the two spacecraft, the greater is the uncertainty in the deduced speed (becoming uncertain at less than about 120000 km, and insoluble at zero separation),

2. The greater the radial separation of the two spacecraft, the less will B_z remain sufficiently coherent to give an adequate correlation (though compensated by (4) to some extent),

3. There are no constraints on angular separation, even if the spacecraft are on the same helio-meridian (though the coherence limit in (2) still applies),

4. The more intense the activity (e.g. very fast solar wind streams and energetic CMEs) the more structure is likely to be present in the IMF and the more likely is an adequate correlation with increased spacecraft separation (both angular and radial).

Given these conditions, the method provides a means of determining the speed of the solar wind particle flux using measurements of the flux density of the magnetic field. This would be useful in situations when particle data is not available, such as in cases of instrument failure, or sensor saturation during very energetic CME events, when magnetometers continue to function. However, given the requirement that a pair of spacecraft with the above separation constraints are required, it is accepted that such occasions will inevitably be infrequent.

Tests have shown that there is insufficient coherent structure in the slow solar wind for this method to be applicable.

9 Acknowledgements

The groundwork for this paper originated during the author's PhD studies, supervised by Dr. B.J.I. Bromage (now deceased). Though not involved with the data analysis and preparation of this paper, Dr. Bromage was instrumental in the early research and is hereby given full recognition for her supervision and scientific contribution.

The authors wish to thank NASA GSFC for the provision of the ACE and Wind data used in this study.

References

Balogh, A., Beek, T.J., Forsyth, R.J., Hedgecock, P.C., Marquedant, R.J., Smith, E.J., Southwood, D.J., Tsurutani, B.T., 1992. The magnetic field investigation on the ULYSSES mission - Instrumentation and preliminary scientific results. Astron. Astrophys. Suppl. Ser. 92 (2), 221-236 (ISSN 0365-0138).

Bian, N.H., Li, G., Stochastic Parker Spirals in the Solar Wind, The Astrophysical Journal, 908:45 (14pp), https://doi.org/10.3847/1538-4357/abd39a, 2021.

Bian, N.H., Li, G., Transport of Solar Energetic Particles along Stochastic Parker Spirals, The Astrophysical Journal, 924:120 (14pp), https://doi.org/10.3847/1538-4357/ac2fab, 2022.

Biermann, L., Kometenschweife und solare Korpuskularstrahlung, Zeitschrift fur Astrophysik, vol.29, p.274-286, January, 1951.

Bravo, S., Stewart, G.A., Fast and Slow Wind from Solar Coronal Holes, Astrophysical Journal, vol.489, p.992, November 1997.

Chapman, S., On the Origin of the Aurora Polaris, Physical Review, vol.32, iss.6, p.993-995, December, 1928.

Chapman, S., Aller, L.H., Diffusion in the sun, Astronomical Journal, vol.64, p.126, 1959.

Chapman, S., Ferraro, V.C.A., The electrical state of solar streams of corpuscles, Monthly Notices of the Royal Astronomical Society, vol.89, p.470, March, 1929.

Cranmer, S, Coronal holes and the high-speed solar wind, Space Science Reviews, vol.101, pp.229-294, 2002.

Cranmer, S., Coronal holes, Living Reviews in Solar Phys., vol.6, no.3., 2009.

Del Zanna, G.; Bromage, B. J. I., The Elephant's Trunk: Spectroscopic diagnostics applied to SOHO/CDS observations of the August 1996 equatorial coronal hole , Journal of Geophysical Research, Volume 104, Issue A5, p. 9753-9766, 1999.

Einaudi, G., Boncinelli, P., Dahlburg, R.B., (et al). Formation of the slow solar wind in a coronal streamer, J. Geophys. Res. 14(A1), 521534, 1999.

Ferraro, V.C.A., A new theory of magnetic storms: a critical survey, The Observatory, vol.56, p.253-259, 1933.

Hajra, R., Sunny, J.V., Corotating interaction regions during solar cycle 24: a study on characteristics and geoeffectiveness, Solar Physics, 297:30, https://doi.org/10.1007/s11207-022-01962-1, 2022.

Heber, B, T. R. Sanderson T.R., Zhang M, Co-rotating interaction regions, Adv. Space Res. Vol. 23, No. 3, pp. 567-579, 1999

Laitinen, T., Dalla, S., Waterfall, C.O.G., Hutchinson, A., An Analytical Model of Turbulence in Parker Spiral Geometry and Associated Magnetic Field Line Lengths, The Astrophysical Journal, 943:108 (12pp), https://doi.org/10.3847/1538-4357/aca892, 2023.

Lepping, R.P.; Ac?na, M.H.; Burlaga, L.F.; Farrell, W.M.; Slavin, J.A.; Schatten, K.H.; Mariani, F.; Ness, N.F.; Neubauer, F.M.; Whang, Y.C.; Byrnes, J.B.; Kennon, R.S.; Panetta, P.V.; Scheifele, J.; Worley, E.M., The Wind Magnetic Field Investigation, Space Science Reviews, Volume 71, Issue 1-4, pp. 207-229, February 1995.

Lukianova R, Holappa L, Mursula K., Centennial evolution of monthly solar wind speeds: Fastest monthly solar wind speeds from long-duration coronal holes. J Geophys. Res. Space Physics.,122(3):27402747, 2017.

McComas, D.J.; Bame, S.J.; Barker, P.; Feldman, W.C.; Phillips, J.L.; Riley, P.; Griffee, J.W., Solar Wind Electron Proton Alpha Monitor (SWEPAM) for the Advanced Composition Explorer, Space Science Reviews, v. 86, Issue 1/4, p. 563-612, July 1998.

Ofman, L., The origin of the slow solar wind in coronal streamers, Adv.Sp. Res. 33(5), 681688, 2004.

Ogilvie, K.W.; Chornay, D.J.; Fritzenreiter, R.J.; Hunsaker, F.; Keller, J.; Lobell, J.; Miller, G.; Scudder, J.D.; Sittler, E.C., Jr.; Torbert, R.B.; Bodet, D.; Needell, G.; Lazarus, A.J.; Steinberg, J.T.; Tappan, J.H.; Mavretic, A.; Gergin, E., SWE, A Comprehensive Plasma Instrument for the Wind Spacecraft, Space Science Reviews, Volume 71, Issue 1-4, pp. 55-77, February 1995.

Parker, E.N., Dynamics of the Interplanetary Gas and Magnetic Fields, Astrophysical Journal, vol.128, p.664, 1958.

Raouafi, N.E., Matteini, L., Squire, J., Badman, S.T., (plus 54 other authors), Parker Solar Probe: Four Years of Discoveries at Solar Cycle Minimum, Space Science Reviews, 219:8, https://doi.org/10.1007/s11214-023-00952-4, 2023.

Richardson J.D., Paularena K.I., Plasma and Magnetic Field Correlations in the Solar Wind, Jnl. Geophys. Res., vol.106, no.A1, pp.239-251, January 2001.

Smith, C.W.; L'Heureux, J.; Ness, N.F.; Acua, M.H.; Burlaga, L.F.; Scheifele, J., The ACE Magnetic Fields Experiment, Space Science Reviews, v. 86, Issue 1/4, p. 613-632, July 1998.

Snyder, C.W., Mariner Solar Wind Measurement, The Physics of Solar Flares, Proceedings of the AAS-NASA Symposium held 28-30 October, 1963 at the Goddard Space Flight Center,

Greenbelt, MD. Edited by Wilmot N. Hess. Washington DC: National Aeronautics and Space Administration, Science and Technical Information Division, 1964., p.273, January 1964.

Sulistiani, S., Herdiwijaya, D., Solar coronal holes and their geo-effectiveness, J. Physics Conf. Series, 1127(1), 012052, 2019.

Verbanac, G., Vrsnak, B., Veronig, A., et al., Equatorial coronal holes, solar wind high-speed streams, and their geoeffectiveness. Astronomy and Astrophysics, 526(A20), 113, 2011.

Weygand J.M., Mattheus W.H., Dasso S., Kivelson M.G., Correlation and Taylor scale variability in the interplanetary magnetic field fluctuations as a function of solar wind speed, Jnl. Geophys. Res., vol.116, A08102, doi:10.1029/2011JA016621, 2011.